

Radiolabeling of VEGF₁₆₅ with ^{99m}Tc to evaluate VEGFR expression in tumor angiogenesis

FILIPPO GALLI^{1,2*}, MARCO ARTICO^{3*}, SAMANTA TAURONE³, ISABELLA MANNI⁴,
ENRICA BIANCHI³, GIULIA PIAGGIO⁴, BRUCE D. WEINTRAUB⁵, MARIUSZ W. SZKUDLINSKI⁵,
ENZO AGOSTINELLI⁶, RUDI A.J.O. DIERCKX² and ALBERTO SIGNORE^{1,2}

¹Nuclear Medicine Unit, Department of Medical-Surgical Sciences and of Translational Medicine, Faculty of Medicine and Psychology, 'Sapienza' University of Rome, Rome, Italy; ²Department of Nuclear Medicine and Molecular Imaging, University Medical Centre Groningen, University of Groningen, Groningen, The Netherlands; ³Department of Sensory Organs, 'Sapienza' University of Rome; ⁴SAFU UOSD, Department of Research, Advanced Diagnostics and Technological Innovation, Regina Elena National Cancer Institute, Rome, Italy; ⁵Trophogen Inc., Rockville, MD, USA; ⁶Department of Biochemical Sciences 'A. Rossi Fanelli', 'Sapienza' University of Rome, Rome, Italy

Received December 3, 2016; Accepted March 27, 2017

DOI: 10.3892/ijo.2017.3989

Abstract. Angiogenesis is the main process responsible for tumor growth and metastatization. The principal effector of such mechanism is the vascular endothelial growth factor (VEGF) secreted by cancer cells and other components of tumor microenvironment. Radiolabeled VEGF analogues may provide a useful tool to noninvasively image tumor lesions and evaluate the efficacy of anti-angiogenic drugs that block the VEGFR pathway. Aim of the present study was to radiolabel the human VEGF₁₆₅ analogue with ^{99m}Technetium (^{99m}Tc) and to evaluate the expression of VEGFR in both cancer and endothelial cells in the tumor microenvironment. ^{99m}Tc-VEGF showed *in vitro* binding to HUVEC cells and *in vivo* to xenograft tumors in mice (ARO, K1 and HT29). By comparing *in vivo* data with immunohistochemical analysis of excised tumors we found an inverse correlation between ^{99m}Tc-VEGF₁₆₅

uptake and VEGF histologically detected, but a positive correlation with VEGF receptor expression (VEGFR1). Results of our studies indicate that endogenous VEGF production by cancer cells and other cells of tumor microenvironment should be taken in consideration when performing scintigraphy with radiolabeled VEGF, because of possible false negative results due to saturation of VEGFRs.

Introduction

Angiogenesis is the vital physiological process involving the growth and remodeling of new blood vessels and is implicated in a number of diseases including cancer. Neoangiogenesis is essential for tumor growth as well as crucial for local and distant metastatization through both blood and lymphatic vessels (1,2). Therefore, many new targeted therapies have been developed and they are based on drugs able to bind vascular endothelial growth factor (VEGF) and its receptor (VEGFR), which have been shown to be upregulated in tumor and highly proliferating endothelial cells. Such overexpression has been associated with progression, metastatization and poor outcome in particularly aggressive cancers (3,4). Some of these drugs have been approved for human use and proved to be effective in many solid tumors (5).

The most widely used in clinical practice is the anti-VEGF monoclonal antibody (mAb) bevacizumab that binds the free VEGF. Others, like the tyrosine kinase inhibitors (TKIs) sorafenib and sunitinib, are able to target the VEGFR2 blocking the signaling cascade (6). It has been reported that the majority of patients benefits from targeted therapies, but a small fraction fails to show even initial benefits. The reasons may range from the involvement of parallel angiogenic pathways to the absence of the targets (7). Therefore, it would be important to predict which patients would benefit from a specific targeted therapy and several studies indicated the possibility to image angiogenic markers with the use of radiopharmaceuticals targeting VEGF or VEGFR (8).

Correspondence to: Dr Filippo Galli, Nuclear Medicine Unit, 'Sapienza' University of Rome, St. Andrea Hospital, Via di Grottarossa 1035, I-00189 Rome, Italy
E-mail: filippo.galli@hotmail.com

*Contributed equally

Abbreviations: FCS, fetal calf serum; HRC, high-resolution portable mini-gamma camera; HYNIC, 6-hydrazinonicotinamide; ITLC, instant thin layer chromatography; LE, labeling efficiency; mAb, monoclonal antibody; MES, 2-(N-morpholino) ethanesulfonic acid; PBS, phosphate buffered saline; ^{99m}Tc, ^{99m} Technetium; TKI, tyrosine kinase inhibitors; VEGF, vascular endothelial growth factor; VEGFR, vascular endothelial growth factor receptor

Key words: VEGF, nuclear medicine, angiogenesis, preclinical imaging, oncology

In particular, since VEGFR is expressed also in some cancer cells, this technique will be useful in both early detection and cancer treatment monitoring (9-12). Radiopharmaceuticals to image tumor angiogenesis have been described in the literature, but many of them showed limitations that slowed or blocked the shift from preclinical to clinical trials (13). Among them the most common were poor or variable binding affinity and exaggerated liver uptake (14,15). In the present study, we optimized the radiolabeling of VEGF₁₆₅ with ^{99m}Tc using HYNIC as bifunctional chelator, obtaining a highly stable radiopharmaceutical with high *in vitro* receptor binding affinity. *In vivo* we used ^{99m}Tc-HYNIC-VEGF₁₆₅ to image VEGFR expression in different tumor xenografts and correlated *in vivo* data with histological findings.

Materials and methods

Radiolabeling of VEGF-A165 with ^{99m}Tc. The human VEGF-A165 analogue with a molecular weight of 19 kDa was provided by Trophogen Inc. and radiolabeled with ^{99m}Tc through an indirect method after conjugation with the bifunctional chelator 6-hydrazinonicotinamide (HYNIC).

Radiolabeling was optimized by testing several labeling conditions including different HYNIC:VEGF ratios (1:1, 4:1 and 8:1) and different amounts of tricine (from 0.9 mg/ml to 200 mg/ml PBS) or SnCl₂ (from 2 mg/ml to 20 mg/ml 0.1 M HCl). Briefly, VEGF₁₆₅ (0.5 mg) was incubated with an excess of succinimidyl-6-hydrazinonicotinate hydrochloride (SHNH, SoluLink Inc., San Diego, CA, USA) for 2 h at room temperature in the dark. At the end of the incubation free SHNH was removed by size exclusion chromatography using a G-25 Sephadex PD10 column (GE Healthcare, Little Chalfont, Buckinghamshire, UK) and nitrogen-purged phosphate buffer saline (pH 7.4) as eluent.

The number of HYNIC groups bound per molecule of VEGF₁₆₅ was determined by a molar substitution ratio (MSR) assay. Briefly, conjugated VEGF₁₆₅ (2 μl) was added to a 0.5 mM solution (18 μl) of 2-sulfobenzaldehyde in 0.1 M 2-(*N*-morpholino) ethanesulfonic acid (MES) buffer (pH 5.0) and incubated at room temperature for 2 h. Phosphate buffer saline (PBS) alone was used as blank and duplicates were prepared. After 2 h the absorbance at 345 nm of each reaction was measured with a spectrophotometer and the number of HYNIC groups per molecule was calculated as indicated in the SoluLink data sheet. Radiolabeling was performed incubating 30 μg of VEGF₁₆₅ (in 100 μl PBS) with 300 MBq of freshly eluted ^{99m}TcO₄⁻ (100 μl), 100 μl of tricine (Sigma-Aldrich Chemicals, Dorset, UK) and 5 μl SnCl₂ (Sigma-Aldrich Chemicals). Labeling efficiency (LE) and colloids percentage were measured up to 30 min of incubation. After labeling, an additional purification by size exclusion chromatography was performed using a Zeba Spin Column (Thermo Fisher Scientific, Waltham, MA, USA) to remove any free ^{99m}TcO₄⁻, tricine and SnCl₂.

***In vitro* quality controls.** Quality controls were performed using instant thin layer chromatography-silica gel (ITLC-SG) strip (Pall Life Sciences, Port Washington, NY, USA). Results were analyzed by a radio scanner (Bioscan Inc., Washington, DC, USA) to calculate the LE of ^{99m}Tc-HYNIC-VEGF₁₆₅. The mobile phase for LE determination was a 0.9% NaCl solution, whereas the amount of colloids was determined using

a NH₃:H₂O:EtOH (1:5:3) solution. Quality controls were performed before and after the purification with a Zeba Spin column. Additionally, reverse phase HPLC was carried out using a C8 Kinetex 4.6x250 mm column and a gradient of H₂O (A) and acetonitrile (B) with 0.1 % TFA. The following gradient was used: 0-5 min 0-5% B, 5-20 min 5-95% B, 20-25 min 95% B and 25-30 min 95-5% B. Stability assays were performed adding 100 μl of ^{99m}Tc-HYNIC-VEGF₁₆₅ to a vial containing 900 μl of fresh human blood serum and to another containing 900 μl of 0.9% NaCl solution. Both vials were incubated up to 24 h at 37°C. The radiochemical purity was measured at 1, 3, 6 and 24 h by ITLC analysis. A cysteine challenge assay was performed incubating the radiolabeled VEGF₁₆₅ at 37°C for 60 min with different cysteine concentration, ranging from 1000:1 (cysteine:VEGF₁₆₅) to 0.1:1 molar ratio. For each time point, radiochemical purity was evaluated by ITLC as described above. All known chemical forms of ^{99m}Tc-cysteine have Rf values between 0.5 and 1, when normal saline was used as mobile phase.

Integrity of the radiolabeled VEGF₁₆₅ molecule was also checked by sodium dodecyl sulphate-polyacrylamide gel electrophoresis under non-reducing conditions, according to the method of Laemmli (16). Proteins were visualized by staining the gels with Coomassie Brilliant Blue (Thermo Fisher Scientific). Radioactivity associated with each band was determined scanning the gel with a radio scanner.

Cell lines. VEGFR⁺ cell line, human umbilical veins endothelial cells (HUVEC) were cultured in F-12K medium supplemented with 10% FCS, 100 IU/ml penicillin, 100 μg/ml streptomycin, 2 mM L-glutamine and EGM[®]-2 Bullet kit (Lonza, Walkersville, MD, USA) (17). The human anaplastic thyroid cancer cell line (ARO), the human colorectal cancer cell line (HT29) and the human poorly differentiated thyroid cancer cell line (K1) were grown in DMEM high glucose (Gibco, Carlsbad, CA, USA) supplemented with 10% FCS, 100 IU/ml penicillin, 100 μg/ml streptomycin and 2 mM L-glutamine (18-20).

In vitro binding studies. Measurements of cell uptake and retention of radiolabeled VEGF-A165, was performed *in vitro* using the semi-automatic system LigandTracer[™] that allows to follow binding over time (Ridgeview Instruments AB, Vänge, Sweden) (21). Briefly, 10⁶ HUVEC cells were seeded in a tilted Petri dish and incubated in a humidified incubator at 37°C and 5% CO₂ for 24 h. The dish was then placed in the LigandTracer and allowed to rotate continuously for 15 min to induce the release of weakly attached cells. After one gentle wash, 2 ml of PBS containing radiolabeled VEGF₁₆₅ (30 nM) were added to the dish and the rotation started, and the device was stopped when reaching maximal binding. Then the liquid was removed and replaced with culture medium without radiolabeled VEGF₁₆₅ for calculating release of radioactivity from cells. Association and dissociation curves were obtained analyzing data by non-linear regression analysis with GraphPad Prism (GraphPad Software Inc., La Jolla, CA, USA) to calculate the k_{on}, k_{off} and K_d values.

In vivo studies

Biodistribution and imaging studies. For animal experiments, approval of the local ethics committee was obtained and the

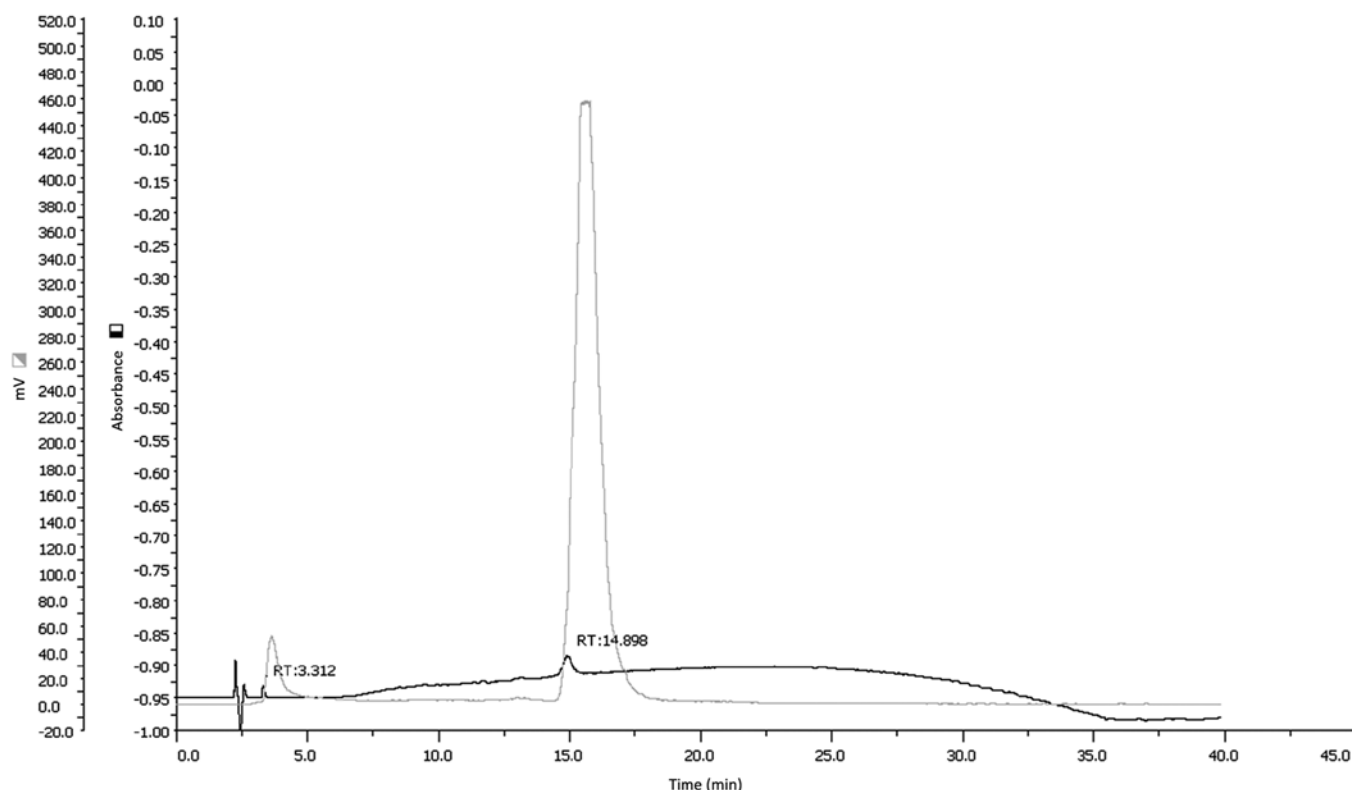


Figure 1. HPLC profile showing UV (black) and radioactive (grey) chromatograms of ^{99m}Tc -HYNIC-VEGF₁₆₅.

institutional and national guide for the care and use of laboratory animals was followed. Imaging studies were performed with a previously described high-resolution portable mini-gamma camera (HRC), IP-Guardian (Li-Tech S.r.l., Italy) (22). For *in vivo* biodistribution studies, 5.5 MBq (190 MBq/nmol, 100 μl) of radiolabeled VEGF₁₆₅ were injected in the tail vein of 12 nude CD-1 mice and static planar posterior images were acquired using the HRC at 1, 3, 6 and 24 h, under light ether anesthesia. At the end of each imaging point three mice were euthanized and major organs were collected and counted in a single well gamma-counter.

In vivo cell-targeting experiments were performed in 36 nude CD-1 mice that were divided in three groups. Each group was injected subcutaneously in the right thigh with respectively 10⁶ ARO, HT29 and K1 cells mixed with BD Matrigel® (BD Biosciences, Franklin Lakes, NJ, USA) (1:1). After tumor growth (approximately 0.6-1 cm³, in 20 days), 5.5 MBq of radiolabeled VEGF₁₆₅ were administered i.v. in the tail vein and static planar posterior HRC images were acquired at 1, 3, 6 and 24 h, under light ether anesthesia. At each time point 3 mice were euthanized for *ex vivo* counting. Major organs and tumors were collected, weighed and counted for radioactivity with a single well gamma-counter (Gammatom, Italy).

Blocking studies. Blocking studies were performed in four mice injected with 1 million HT29 cells mixed with Matrigel in the right thigh. After tumor growth, 5.5 MBq of ^{99m}Tc -VEGF₁₆₅ were injected in the tail vein and images were acquired with a portable mini-gamma camera at 1 and 3 h post-injection. After 3 days, ^{99m}Tc -HYNIC-VEGF₁₆₅ was pre-incubated for 1 h with 3.5-fold molar excess of recombinant human VEGFR2-Fc

chimera (BioLegend Inc., San Diego, CA, USA) that act as a soluble decoy receptor (TRAP) that has been proved to prevent the binding of VEGF to endothelial cells. After the incubation, a dose of 5.5 MBq was injected in the tail vein of 3 of the 4 mice previously imaged and images were acquired with a portable mini-gamma camera at 1 and 3 h post-injection. After 3 more days, a 100-fold molar excess of unlabeled VEGF₁₆₅ (COLD) was injected in the tail vein of the same 3 mice and after 10 min 5.5 MBq of ^{99m}Tc -HYNIC-VEGF₁₆₅ was injected. Images were acquired with a portable mini-gamma camera at 1 and 3 h post-injection. Region of interest were drawn on the tumor and on the contralateral leg in each image and target-to-background (T/B) ratios were calculated.

Immunohistochemical analysis. For light microscope immunohistochemical analysis, small fragments of each excised tumor (ARO, HT29 and K1) were processed according to ABC/HRP technique (avidin-complexed with biotinylated peroxidase). These samples were washed in PBS, fixed in 10% formalin and embedded in paraffin according to a standard procedure. Serial 3- μm sections were cut using a rotating microtome, mounted on gelatin-coated slides and processed for immunohistochemistry. These sections were de-paraffinized in xylene and dehydrated. They were immersed in citrate buffer (pH 6.0) and subjected to microwave irradiation twice for 5 min. Subsequently, all sections were treated for 30 min with 0.3% hydrogen peroxide in methanol to quench endogenous peroxidase activity. To block non-specific binding, the slides were incubated with M.O.M. Mouse Ig Blocking Reagent (Vector Laboratories Burlingame, Burlingame, CA, USA) for 1 h at room temperature. The slides were incubated overnight at 4°C

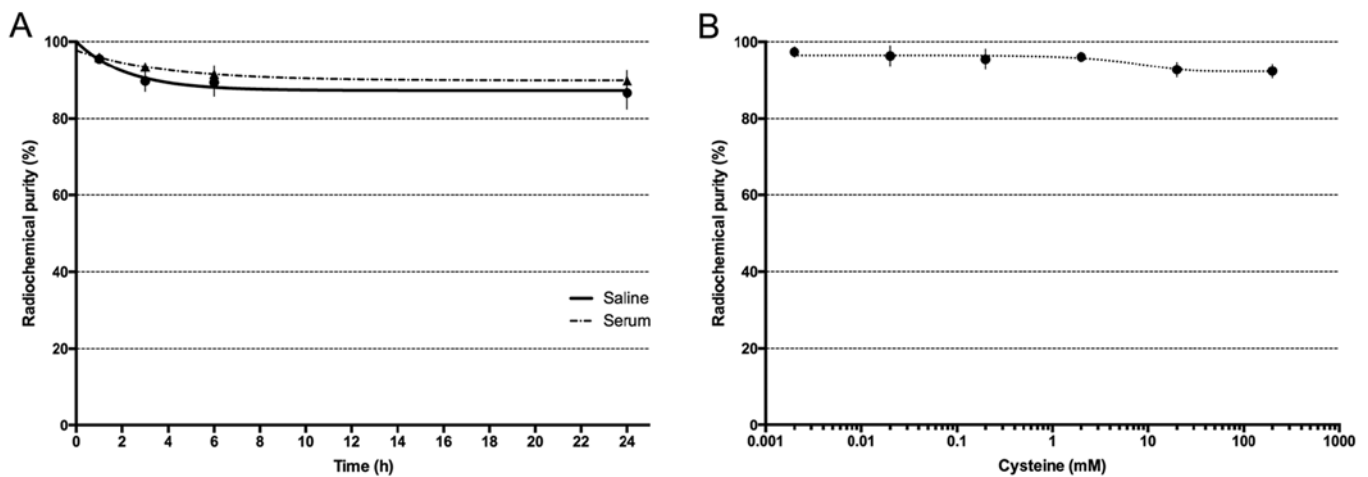


Figure 2. Stability assay performed in saline and human serum (A), and cysteine challenge (B) of ^{99m}Tc-HYNIC-VEGF₁₆₅.

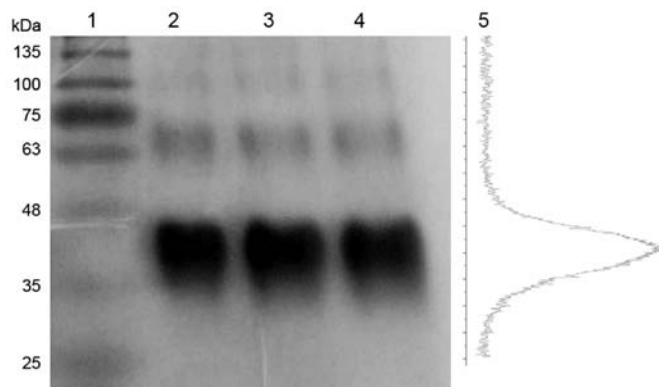


Figure 3. SDS-Page electrophoresis in non-reducing conditions showing native (2), conjugated (3) and radiolabeled VEGF₁₆₅ (4). Lanes 1 and 5 represent the molecular weight marker and scan of well no. 4 with a linear radioactivity scanner.

with the following antibodies: i) mouse anti-VEGF monoclonal antibody (Santa Cruz Biotechnology, Santa Cruz, CA, USA); ii) mouse anti-VEGF receptor 1 (Flt-1/EWC) monoclonal antibody (ab9540; Abcam, Cambridge, UK); iii) mouse anti-VEGF Receptor 2 (KDR/EIC) monoclonal antibody (ab9530; Abcam). Optimal antisera dilutions and incubation times were assessed in a series of preliminary experiments. After exposure to the primary antibodies, slides were rinsed twice in phosphate buffer and incubated for 1 h at room temperature with the appropriate secondary biotinylated goat anti-mouse IgG (Vector Laboratories Burlingame, BA9200 and BA1000) and with peroxidase-conjugated avidin (Vectastain Elite ABC kit standard PK 6-100) for 35 min. After a further wash with phosphate buffer, slides were treated with 0.05% 3,3-diaminobenzidine (DAB) and 0.1% H₂O₂ (DAB substrate kit for peroxidase, Vector Laboratories SK-4100). Finally, sections were counterstained with Mayer's haematoxylin and observed using a light microscope.

Negative control experiments were carried out: i) by omitting the primary antibody; ii) by substituting the primary antibody with an equivalent amount of non-specific immunoglobulins; iii) by pre-incubating the primary antibody with the specific

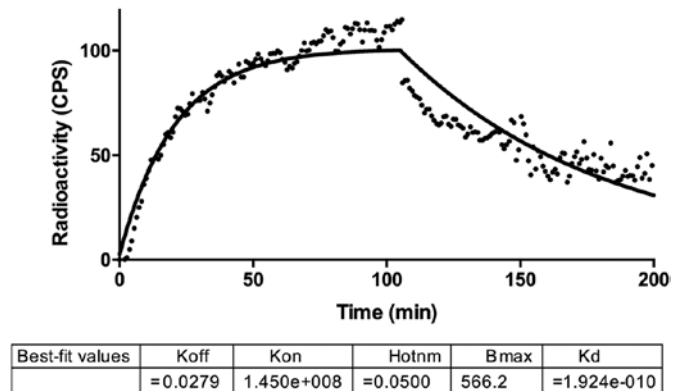


Figure 4. Kinetic binding assay of radiolabeled VEGF₁₆₅ on HUVEC cells. Fitting was obtained by nonlinear regression analysis determining k_{on} (1.45×10^8), k_{off} (0.0279) and k_D (192 pM).

blocking peptide (antigen/antibody = 5 according to supplier's instructions). The staining assessment was made by two experienced observers in light microscopy. Immunoreactivity of VEGF, VEGFR1, and VEGFR2 was assessed in all samples. The intensity of the immune reaction was assessed microdensitometrically using an IAS 2000 image analyzer (Delta Sistemi, Rome, Italy). The system was calibrated taking as zero the background obtained in sections exposed to non-immune serum. Ten 100 μm^2 areas were delineated in each section using a measuring diaphragm. The quantitative data regarding the intensity of immune staining were analyzed statistically using analysis of variance (ANOVA) followed by Duncan's multiple range test as a post-hoc test.

Results

VEGF₁₆₅ analogue can be efficiently radiolabeled with ^{99m}Tc. Highest labeling efficiency was obtained when the analogue was conjugated with a ratio HYNIC:VEGF₁₆₅ of 8:1. Determination of molar substitution ratio of HYNIC-conjugated VEGF₁₆₅ demonstrated that an average of 4.3 molecules of HYNIC groups were bound per molecule of analogue. Higher ratios were not selected to avoid over-conjugation of the hormone and

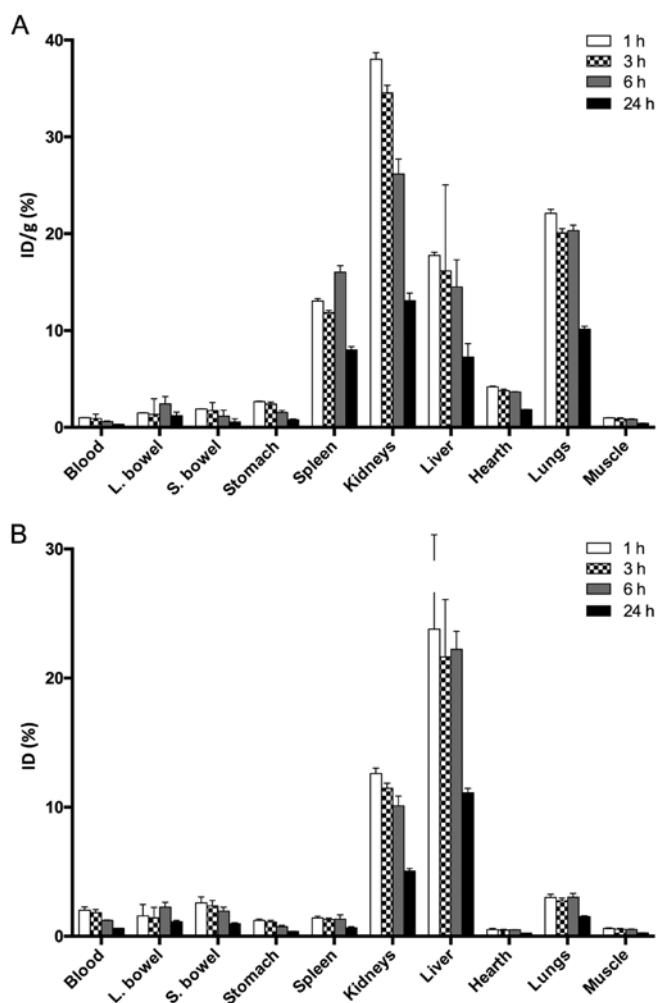


Figure 5. Single organ counts at 1 h (white bars), 3 h (squared bars), 6 h (grey bars), and 24 h (black bars). Data are shown as %ID/g (A) and %ID/organ (B) over time. Each point is the mean of three mice. Error bars represent standard deviation.

possible structural modification. Optimization of the labeling procedure of the HYNIC-VEGF₁₆₅ conjugate (30 μg) with ^{99m}Tc showed that, after 10 min of incubation, the use of 100 μl of tricine (0.5 mM) and 5 μl of SnCl₂ (50 nM) allowed to obtain the highest LE (65%) and the lowest amount of colloids (<5%). After purification we were able to obtain a radiochemical purity of >95% as confirmed by both ITLC and HPLC analysis (Fig. 1). Specific activity of resulting ^{99m}Tc-HYNIC-VEGF₁₆₅ was 190 MBq/nmol. Radiolabeled VEGF₁₆₅ was stable up to 24 h in both in human serum and in a 0.9% NaCl solution at 37°C, as well as in solutions containing increasing cysteine concentrations (Fig. 2A). A slight decrease in the radiochemical purity was observed only at high cysteine concentrations (>500:1) (Fig. 2B). Gel electrophoresis of radiolabeled, conjugated and unconjugated analogue showed no significant differences and the absence of significant degradation or aggregation resulting from conjugation and/or labeling (Fig. 3). Poor resolution of the bands is due to the high glycosylation of the analogues.

Radiolabeled VEGF₁₆₅ binds with high affinity to VEGFRs. Kinetic binding assay with LigandTracer showed an increasing uptake of radiolabeled VEGF₁₆₅ from HUVEC cells that

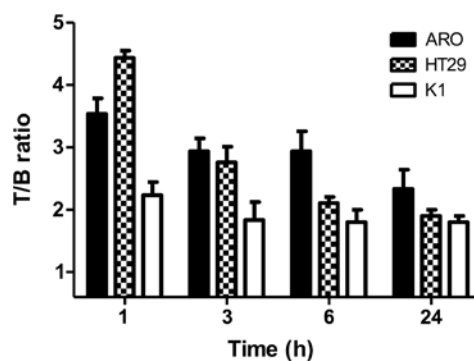


Figure 6. T/B ratios calculated at 1, 3 and 6 h in mice bearing an ARO (black bars), HT29 (squared bars) or K1 (white bars) xenograft. Each point is the mean of three mice. Error bars represent standard deviation.

reached a plateau after 50 min (Fig. 4). Retention studies revealed a slow dissociation rate from membrane bound receptors in the following 2 h, with a K_d of 192 pM.

^{99m}Tc-HYNIC-VEGF₁₆₅ is able to image tumor xenografts in mice. Biodistribution studies with ^{99m}Tc-HYNIC-VEGF₁₆₅ showed a high and persistent uptake by the liver and a moderate uptake by the kidneys with almost no signal from other organs and blood pool (Fig. 5). Single organ counting revealed a high %ID/g also in the lungs and spleen. *In vivo* targeting experiments showed a focal uptake in the right thigh of each group bearing tumor xenografts with a T/B ratio of 4.5 at 1 h p.i in mice bearing a HT29 xenograft. Animals bearing ARO and K1 cells showed a T/B of 3.5 and 2.3, respectively, that decreased over time (Fig. 6).

In vivo binding of ^{99m}Tc-HYNIC-VEGF₁₆₅ can be inhibited by an excess of unlabeled VEGF or VEGFR2-Fc. Blocking studies with ^{99m}Tc-HYNIC-VEGF₁₆₅ confirmed the results of previous targeting experiments. After pre-incubation of the radiopharmaceutical with recombinant VEGFR2-Fc, a main liver and spleen uptake, with reduced signal from kidneys, was detected, resembling the typical biodistribution of a non-specific radiolabeled antibody (Fig. 7). The overall uptake in tissues was lower and the uptake in the tumor was considerably reduced. Similar findings were obtained after the pre-injection of a 100-fold molar excess of unlabeled VEGF₁₆₅ with the exception of the signal from kidneys, which was similar to the signal obtained with labeled VEGF only. Calculated T/B ratios for the 'HOT' group reflected the data obtained with the previous experiments with a maximum uptake reached at 1 h that slowly decreases with time (Fig. 8). The T/B ratio in the TRAP group was reduced by 70% due to the co-incubation with VEGFR2-Fc at 1 h and the T/B ratio in the 'COLD' group was reduced by 60% at 1 h. Minor blocking was evident at 3 h in both TRAP and 'COLD' group mainly due to the decreased activity in tumors of the control group.

VEGF expression at IHC and T/B ratio of ^{99m}Tc-HYNIC-VEGF₁₆₅ correlates inversely. IHC analysis on excised tumor showed the presence of VEGF, VEGFR1 and VEGFR2 on both the lesion and the surrounding vessels to different extent (Fig. 9). After semi-quantitative analysis of expression levels,

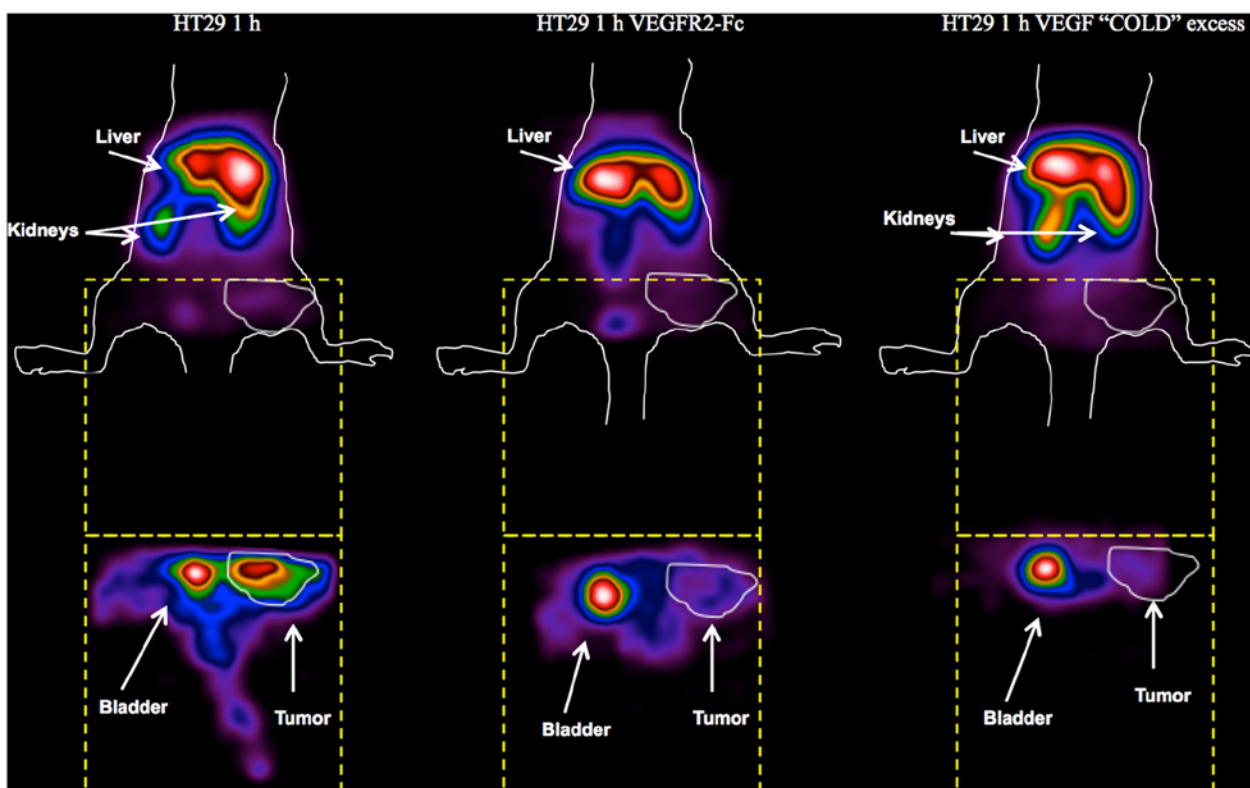


Figure 7. Body images (top) and details of the back (bottom) of the same mouse injected with 5.5 MBq of ^{99m}Tc-VEGF (left), 5.5 MBq of ^{99m}Tc-VEGF following pre-incubation with a 3.5-fold molar excess of VEGFR2-Fc (middle) and 5.5 MBq of ^{99m}Tc-VEGF following pre-injection of a 100-fold molar excess of unlabeled VEGF (right).

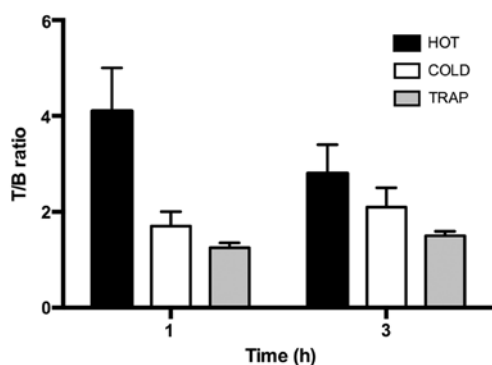


Figure 8. T/B ratios at 1 and 3 h calculated on the images obtained from the HOT (^{99m}Tc-VEGF), COLD (^{99m}Tc-VEGF+unlabeled VEGF) and TRAP (^{99m}Tc-VEGF+VEGFR2-Fc) groups. Values are the mean of 3 mice per each group and images were acquired at 1 h p.i. Error bars represent standard deviation.

a higher amount of free VEGF was present in lesions derived from K1 cell lines (33.2%), followed by HT29 (15.7%) and ARO cells (10.6%). VEGFR1 and -2 were present heterogeneously between tumor cells and blood vessels, revealing that even cancer may express VEGF receptors on the plasma membrane. IHC data were compared with the uptake of radioactive VEGF₁₆₅ and an inverse correlation was observed between endogenous VEGF and T/B ratio ($r^2=0.63$; $p=0.03$, Fig. 10A). On the contrary, a positive correlation was observed between radioactive VEGF₁₆₅ uptake and VEGFR1 ($r^2=0.64$; $p=0.03$, Fig. 10B). In addition, tumor weight positively corre-

lates with VEGF production ($r^2=0.65$; $p=0.03$) and shows a trend to inversely correlate with radiolabeled VEGF uptake ($r^2=0.31$; $p=0.35$).

Discussion

Imaging of tumor microenvironment has been described as a promising approach for non-invasive diagnosis of cancer metastases and to monitor the efficacy of new drugs (23). Given the role of angiogenesis in metastatization and tumor growth, VEGF and its receptors are optimal diagnostic and therapeutic targets (24). Their presence has been reported in many cancer types and it was correlated with clinical data. However, given the heterogeneity of VEGFR expression on cancer cells, their role in tumor dedifferentiation or signaling is still unclear (13). In undifferentiated thyroid cancer, the use of TKIs blocking the VEGF/VEGFR pathway showed its potential as a promising therapeutic approach (25). Unfortunately, severe side effects have been reported in some patients after long time treatment. Therefore, a non-invasive diagnostic tool to predict the response to therapy and evaluate drug efficacy is vitally needed. In the past many attempts have been made to develop radiopharmaceuticals to image angiogenesis with promising results. Among them, ¹¹¹In, ⁸⁹Zr or ⁶⁴Cu radiolabeled bevacizumab was able to efficiently image xenografts from ovarian cancer, but the high radiation burden to the patient and the low availability of ⁸⁹Zr and ⁶⁴Cu were some of the drawbacks of its use (26,27).

Other groups tried to use recombinant human VEGF to overcome the long half-life of mAbs and used radio-

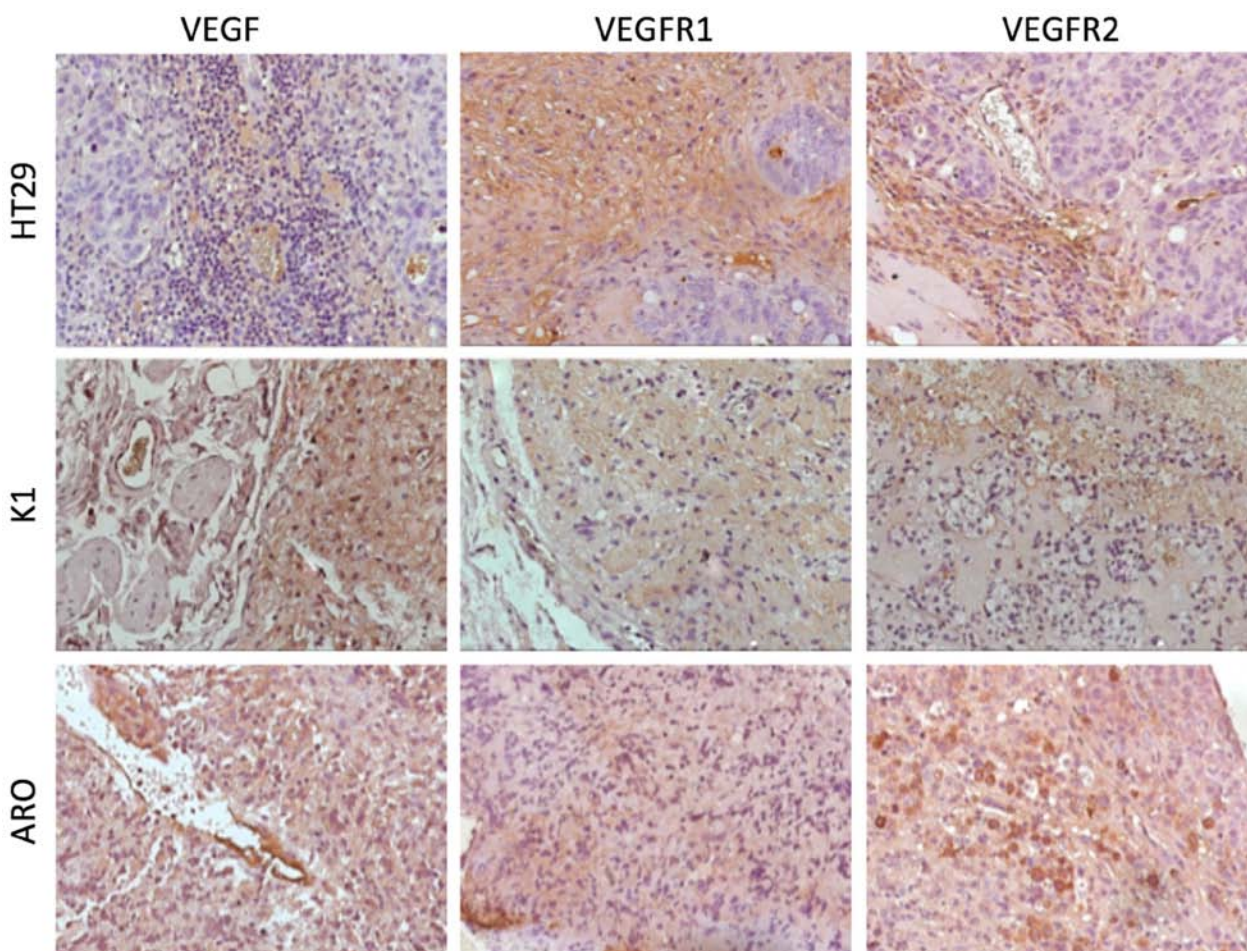


Figure 9. IHC analysis of VEGF, VEGFR1 and VEGFR2 expression on HT29, K1 and ARO excised tumors.

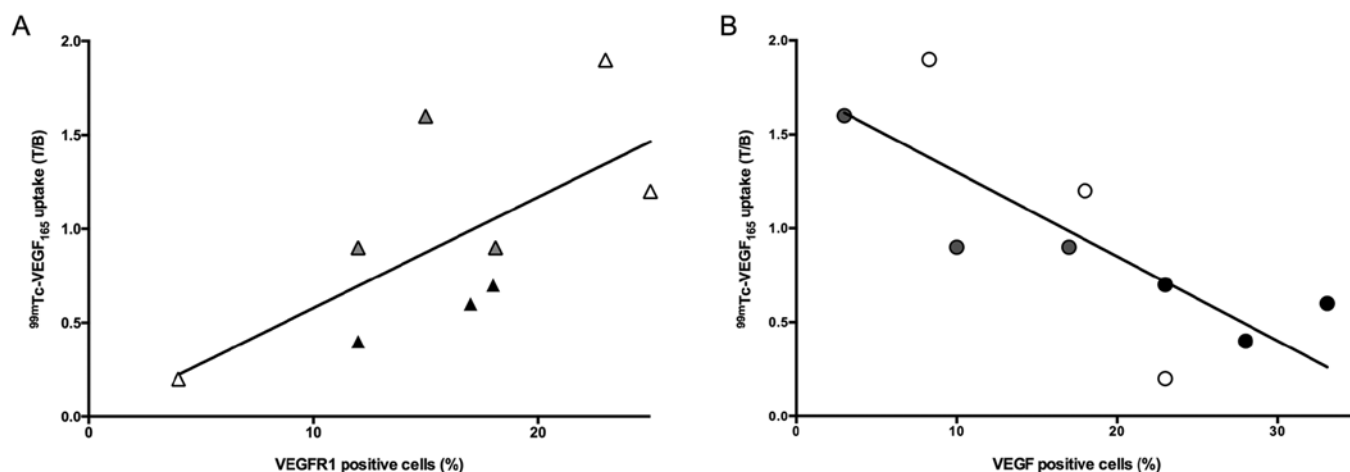


Figure 10. Correlation between ^{99m}Tc -VEGF₁₆₅ uptake and VEGFR1 positive cells (%) (A) and between ^{99m}Tc -VEGF₁₆₅ uptake and VEGF positive cells (%) (B) in ARO (grey), HT29 (white) and K1 (black) cell lines.

iodine, ^{99m}Tc (Technetium (^{99m}Tc), ^{64}Cu or ^{68}Ga as the isotopes of choice (8,13). In the present study, we followed the same approach to strengthen the hypothesis that the use of recombinant human VEGF to target angiogenesis is a promising methodology to develop non-invasive diagnostic tools and monitor novel targeted drug development. In addition we improved the radiolabeling method to produce a high specific

activity and highly stable radiopharmaceutical to bind VEGFR with high binding affinity and avoid misinterpretation of *in vivo* studies. Furthermore, the use of picomolar amounts of radiolabeled VEGF for a scintigraphic study should not raise any concern about a potential biologic effect of such radiopharmaceuticals and in particular on the pro-angiogenic effect that VEGF analogues may have on existing blood vessels.

Thus, *in vivo* results allowed us to image tumor angiogenesis in xenografts from three different human cell lines with high T/B ratio between 1 and 3 h post-injection (max T/B at 1 h for HT29 was 4.5). Nevertheless a high liver uptake was observed in all mice till late time points, confirming previous findings from other groups (28).

The issue has been raised that VEGF-based probes uptake in the tumor area is highly heterogeneous, probably because of the combination of several mechanisms like non-uniform perfusion of tumor vasculature, differential receptor occupancy by host VEGF or differential accessibility of VEGF receptors on luminal and subluminal surfaces of the endothelium (29,30). Moreover, it has been reported by Chen *et al* that tumor size negatively influences the uptake of radiolabeled VEGF by the tumor, probably because of the presence of necrotic areas (31). To address, in particular, the role of necrosis and endogenous VEGF production, we performed histological and immunohistochemical analysis of each tumor imaged with ^{99m}Tc-VEGF₁₆₅. Results confirmed variability in VEGFR1 and VEGFR2 receptor expression and ligand occupancy in both host endothelium and cancer cells. The presence of both receptors has been also confirmed in a recent study by Meyer *et al*, but it would be of interest to investigate the differential contribution of the different VEGFR subtypes (29). Moreover, we confirm that bigger tumors show lower uptake of radiolabeled VEGF, although we did not observe the presence of significant necrotic areas in any tumor. On the other hand, we observed a positive correlation between tumor size and production of endogenous VEGF (p=0.03), suggesting that the reduced tumor uptake of the radiopharmaceutical could depend on saturation of VEGFRs rather than size or necrosis, as previously suggested (30).

Therefore, this study highlights an important aspect that has not been considered before: the role of both endogenous VEGF production and VEGFR expression on imaging strategies. While for other ligand receptor systems, the endogenous production of the ligand may not be highly relevant for imaging the receptor ligand (i.e. IL-2 and IL-2 receptor) (32,33), herein we show that the high production of endogenous VEGF by tumor cells hampers the possibility to image its receptors. In light of our results we can better interpret previously published studies with radiolabeled VEGF (both VEGF₁₂₁ and VEGF₁₆₅) (34) that showed very poor tumor uptake, in contrast with studies with radiolabeled anti-VEGF mAb that showed high tumor uptake (35). Collectively, these data confirm that the presence of high VEGF levels in tumors, particularly those advanced with highly hypoxic tumor microenvironment and aggressive phenotypes, may saturate VEGF receptors, thus limiting the possibility to image receptors.

Overexpression of soluble VEGFR in some tumors and significant sequestration of VEGF on cell surface heparin-sulfate proteoglycans may also contribute to highly variable imaging results in different tumors. One possible limitation of our study is the limited number of animals used. However, in mice bearing K1 tumors, or ARO or HT29, we found highly consistent data supporting the very low variability within the same cell line. Nevertheless, different tumors showed different levels of VEGF/VEGFR. Another possible limitation could be that the semi-quantitative evaluation of VEGF₁₈₉ that we performed by immunohistochemistry may not represent the

real production of VEGF₁₂₁ and VEGF₁₆₅. However, these forms are splicing variants of the same molecule and are usually expressed in similar quantities (36). Overall we believe that the above considerations may have a limited impact on the final conclusion that VEGFR imaging in tumors by using radiolabeled VEGF is extremely variable, influenced by the presence of endogenous VEGF and unrelated to VEGFR receptor expression. It can be extrapolated that an accurate *in vivo* evaluation of tumor angiogenesis should include both VEGF and VEGFR imaging, unless the predominant clinical relevance of one over the other is demonstrated. Finally, the development of a superagonist VEGF analogue could allow the use of molecule with a greatly increased affinity for its receptor, overcoming the quenching effect due to endogenous VEGF (37).

In conclusion, imaging of angiogenesis by targeting VEGFR with radiolabeled VEGF analogues may be a complementary approach to evaluate angiogenic status of tumors. This approach may allow the evaluation of anti-angiogenic drugs at both preclinical and clinical stages in combination with VEGF imaging. Our results indicate that VEGFR expression is variable in both tumors and its imaging is hampered by endogenous VEGF production. Therefore, additional studies are required to fully understand the VEGF/VEGFR relationship in different cancers and establish a more accurate and angiogenic phenotype-determined imaging protocols.

Acknowledgements

This study was funded by grants from the Italian Association for Cancer Research (AIRC IG-2013 14151 and 13234), 'Sapienza' University research projects and Regione Lazio (FILAS-RU-2014-1020). We also wish to acknowledge the non-profit association Nuclear Medicine Discovery for support.

References

1. Folkman J: Angiogenesis in cancer, vascular, rheumatoid and other disease. *Nat Med* 1: 27-31, 1995.
2. Carmeliet P and Jain RK: Angiogenesis in cancer and other diseases. *Nature* 407: 249-257, 2000.
3. de Araujo-Filho VJ, Alves VA, de Castro IV, Lourenço SV, Cernea CR, Brandão LG and Ferraz AR: Vascular endothelial growth factor expression in invasive papillary thyroid carcinoma. *Thyroid* 19: 1233-1237, 2009.
4. Weidner N, Carroll PR, Flax J, Blumenfeld W and Folkman J: Tumor angiogenesis correlates with metastasis in invasive prostate carcinoma. *Am J Pathol* 143: 401-409, 1993.
5. Hurwitz H, Fehrenbacher L, Novotny W, Cartwright T, Hainsworth J, Heim W, Berlin J, Baron A, Griffing S, Holmgren E, *et al*: Bevacizumab plus irinotecan, fluorouracil, and leucovorin for metastatic colorectal cancer. *N Engl J Med* 350: 2335-2342, 2004.
6. Gruber JJ and Colevas AD: Differentiated thyroid cancer: Focus on emerging treatments for radioactive iodine-refractory patients. *Oncologist* 20: 113-126, 2015.
7. Gotink KJ and Verheul HM: Anti-angiogenic tyrosine kinase inhibitors: What is their mechanism of action? *Angiogenesis* 13: 1-14, 2010.
8. Blankenberg FG, Levashova Z, Sarkar SK, Pizzonia J, Backer MV and Backer JM: Noninvasive assessment of tumor VEGF receptors in response to treatment with pazopanib: A molecular imaging study. *Transl Oncol* 3: 56-64, 2010.
9. Toi M, Inada K, Suzuki H and Tominaga T: Tumor angiogenesis in breast cancer: Its importance as a prognostic indicator and the association with vascular endothelial growth factor expression. *Breast Cancer Res Treat* 36: 193-204, 1995.

10. Folkman J: Angiogenesis: An organizing principle for drug discovery? *Nat Rev Drug Discov* 6: 273-286, 2007.
11. Iagaru A, Chen X and Gambhir SS: Molecular imaging can accelerate anti-angiogenic drug development and testing. *Nat Clin Pract Oncol* 4: 556-557, 2007.
12. Taurone S, Galli F, Signore A, Agostinelli E, Dierckx RA, Minni A, Pucci M and Artico M: VEGF in nuclear medicine: Clinical application in cancer and future perspectives (Review). *Int J Oncol* 49: 437-447, 2016.
13. Goel HL and Mercurio AM: VEGF targets the tumour cell. *Nat Rev Cancer* 13: 871-882, 2013.
14. Dijkgraaf I and Boerman OC: Molecular imaging of angiogenesis with SPECT. *Eur J Nucl Med Mol Imaging* 37 (Suppl 1): S104-S113, 2010.
15. Cai W and Chen X: Multimodality molecular imaging of tumor angiogenesis. *J Nucl Med* 49 (Suppl 2): 113-128, 2008.
16. Laemmli UK: Cleavage of structural proteins during the assembly of the head of bacteriophage T4. *Nature* 227: 680-685, 1970.
17. Zenner HL, Collinson LM, Michaux G and Cutler DF: High-pressure freezing provides insights into Weibel-Palade body biogenesis. *J Cell Sci* 120: 2117-2125, 2007.
18. Ke CC, Liu RS, Yang AH, Liu CS, Chi CW, Tseng LM, Tsai YF, Ho JH, Lee CH and Lee OK: CD133-expressing thyroid cancer cells are undifferentiated, radioresistant and survive radioiodide therapy. *Eur J Nucl Med Mol Imaging* 40: 61-71, 2013.
19. Paudyal B, Paudyal P, Shah D, Tominaga H, Tsushima Y and Endo K: Detection of vascular endothelial growth factor in colon cancer xenografts using bevacizumab based near infrared fluorophore conjugate. *J Biomed Sci* 21: 35, 2014.
20. Challeton C, Branea F, Schlumberger M, Gaillard N, de Vathaire F, Badie C, Antonini P and Parmentier C: Characterization and radiosensitivity at high or low dose rate of four cell lines derived from human thyroid tumors. *Int J Radiat Oncol Biol Phys* 37: 163-169, 1997.
21. Björke H and Andersson K: Automated, high-resolution cellular retention and uptake studies in vitro. *Appl Radiat Isot* 64: 901-905, 2006.
22. Soluri A, Massari R, Trotta C, Montani L, Iurlaro G, Mangano AM, Scopinaro F and Scafè R: New imaging probe with crystals integrated in the collimator's square holes. *Nucl Instrum Methods Phys Res A* 554: 331-339, 2005.
23. Galli F, Iodice V, Lauri C and Signore A: New approaches to image thyroid cancer cells and microenvironment. *Q J Nucl Med Mol Imaging* 59: 184-196, 2015.
24. Stacy MR, Maxfield MW and Sinusas AJ: Targeted molecular imaging of angiogenesis in PET and SPECT: A review. *Yale J Biol Med* 85: 75-86, 2012.
25. Schneider TC, Abdulrahman RM, Corssmit EP, Morreau H, Smit JW and Kapiteijn E: Long-term analysis of the efficacy and tolerability of sorafenib in advanced radio-iodine refractory differentiated thyroid carcinoma: Final results of a phase II trial. *Eur J Endocrinol* 167: 643-650, 2012.
26. Stollman TH, Scheer MG, Franssen GM, Verrijp KN, Oyen WJ, Ruers TJ, Leenders WP and Boerman OC: Tumor accumulation of radiolabeled bevacizumab due to targeting of cell- and matrix-associated VEGF-A isoforms. *Cancer Biother Radiopharm* 24: 195-200, 2009.
27. Van Dongen GA, Huisman MC, Boellaard R, Harry Hendrikse N, Windhorst AD, Visser GW, Molthoff CF and Vugts DJ: 89Zr-immuno-PET for imaging of long circulating drugs and disease targets: Why, how and when to be applied? *Q J Nucl Med Mol Imaging* 59: 18-38, 2015.
28. Blankenberg FG, Backer MV, Levashova Z, Patel V and Backer JM: In vivo tumor angiogenesis imaging with site-specific labeled (99m)Tc-HYNIC-VEGF. *Eur J Nucl Med Mol Imaging* 33: 841-848, 2006.
29. Meyer JP, Edwards KJ, Kozlowski P, Backer MV, Backer JM and Lewis JS: Selective imaging of VEGFR-1 and VEGFR-2 receptors using 89Zr-labeled single-chain VEGF mutants. *J Nucl Med* 57: 1811-1816, 2016.
30. Backer MV, Levashova Z, Patel V, Jehning BT, Claffey K, Blankenberg FG and Backer JM: Molecular imaging of VEGF receptors in angiogenic vasculature with single-chain VEGF-based probes. *Nat Med* 13: 504-509, 2007.
31. Chen K, Cai W, Li ZB, Wang H and Chen X: Quantitative PET imaging of VEGF receptor expression. *Mol Imaging Biol* 11: 15-22, 2009.
32. Signore A, Chianelli M, Annovazzi A, Bonanno E, Spagnoli LG, Pozzilli P, Pallone F and Biancone L: ¹²³I-interleukin-2 scintigraphy for in vivo assessment of intestinal mononuclear cell infiltration in Crohn's disease. *J Nucl Med* 41: 242-249, 2000.
33. Signore A, Capriotti G, Chianelli M, Bonanno E, Galli F, Catalano C, Quintero AM, De Toma G, Manfrini S and Pozzilli P; Action LADA Group: Detection of insulinitis by pancreatic scintigraphy with ^{99m}Tc-labeled IL-2 and MRI in patients with LADA (Action LADA 10). *Diabetes Care* 38: 652-658, 2015.
34. Kang CM, Koo HJ, Choe YS, Choi JY, Lee KH and Kim BT: ⁶⁸Ga-NODAGA-VEGF₁₂₁ for in vivo imaging of VEGF receptor expression. *Nucl Med Biol* 41: 51-57, 2014.
35. Gaykema SB, Brouwers AH, Lub-de Hooge MN, Pleijhuis RG, Timmer-Bosscha H, Pot L, van Dam GM, van der Meulen SB, de Jong JR, Bart J, *et al*: 89Zr-bevacizumab PET imaging in primary breast cancer. *J Nucl Med* 54: 1014-1018, 2013.
36. Cai C, Böttcher MC, Werner JA and Mandic R: Differential expression of VEGF121, VEGF165 and VEGF189 in angiomas and squamous cell carcinoma cell lines of the head and neck. *Anticancer Res* 30: 805-810, 2010.
37. Galli F, Manni I, Piaggio G, Balogh L, Weintraub BD, Szkudlinski MW, Fremont V, Dierckx RA and Signore A: (99m)Tc-labeled-rhTSH analogue (TR1401) for imaging poorly differentiated metastatic thyroid cancer. *Thyroid* 24: 1297-1308, 2014.